MICRO ARCHITECTED POROUS MATERIAL WITH HIGH STRENGTH AND CONTROLLABLE STIFFNESS

James H. Pikul[1], Sezer Ozerinc[1], Runyu Zhang[1], Paul V. Braun[1], and William P. King[1]
[1]University of Illinois at Urbana-Champaign, Urbana, USA

ABSTRACT

This paper reports the engineering of large area cellular solids with controllable stiffness and specific strengths up to 230 MPa/(Mg/m^3), which is stronger than most high strength alloys including 4143 steel and Ti-6Al-4V. The high strength arises from the size-based strengthening of the nm-sized struts. The cellular solid's porosity can be varied from 30 to 90% to control the specific stiffness from 4 – 20 GPa/(Mg/m^3). The cellular solid's regular microporous architecture and self-assembly based fabrication allow nanometer to micrometer control over the hierarchical geometry and chemistry, which enable large area materials with high strength and controllable stiffness.

INTRODUCTION

Materials with continuous nano to macroscale hierarchy have the potential for significant impact by replacing structural materials, such as steel or titanium, with nanoscale cellular solids (NCS), defined by the nm size of the NCS struts, that have strengths approaching their theoretical yield strength, suppress brittle failure, and allow broad chemical functionality [1-3]. Despite significant research activities on NCS, there remains a lack of manufacturing technologies that can control nanoscale structure and chemistry over areas larger than about 5 mm^2 [2, 4, 5].

In this paper, we use self-assembly of µm sized particles to fabricate 2 cm^2 areas of inverse opal NCS with controllable specific moduli between 4 and 20 GPa/(Mg/m^3) and specific strengths up to 230 MPa/(Mg/m^3), which is greater than most high strength alloys including 4143 steel and Ti-6Al-4V. The inverse opal NCS are made flexible or rigid based on the underlying substrate. Micropillar compression tests relate the hierarchical architecture to the bulk strength and stiffness. The combination of self-assembly and near room temperature electrodeposition of nickel and rhenium allow for scalable fabrication of NCS with high specific strength and 10 nm control of structure and chemistry.

METHODS

Figure 1a shows the fabrication of inverse opal NCS. First, a gold coated glass slide (8 nm Cr, 50 nm Au) was immersed in ultrapure water with 3-mercapto-1-propanesulfonic acid, sodium salt (2.2% by weight) for 4 hours and rinsed. The slide was then placed vertically in a 1 inch diameter plastic container filled with a colloidal solution of PS spheres, set on a hot plate at 55 ºC and left until dry, resulting in the self-assembly of PS opals. The PS diameters were varied between 200 – 2,000 nm to change the cellular solid strut size. The substrates were then sintered at 96 ºC for 30 minutes to 6 hours depending on the PS diameter. Longer sinter times increased the interconnect diameter between spheres and reduced the nickel volume fraction. The PS colloidal solution was 8 wt% PS sphere solution (1.2 grams) combined with 40 grams ultrapure water. Nickel was then electrodeposited through the PS opal at a constant -1.8 volts versus a nickel reference electrode for 32 minutes in a commercial plating solution. PS was removed by immersing the substrates in tetrahydrofuran for 24 hours followed by a toluene rinse. The resulting open cell cellular solids were about 15 – 20 µm thick and had interconnected spherical pores arranged in a FCC orientation.

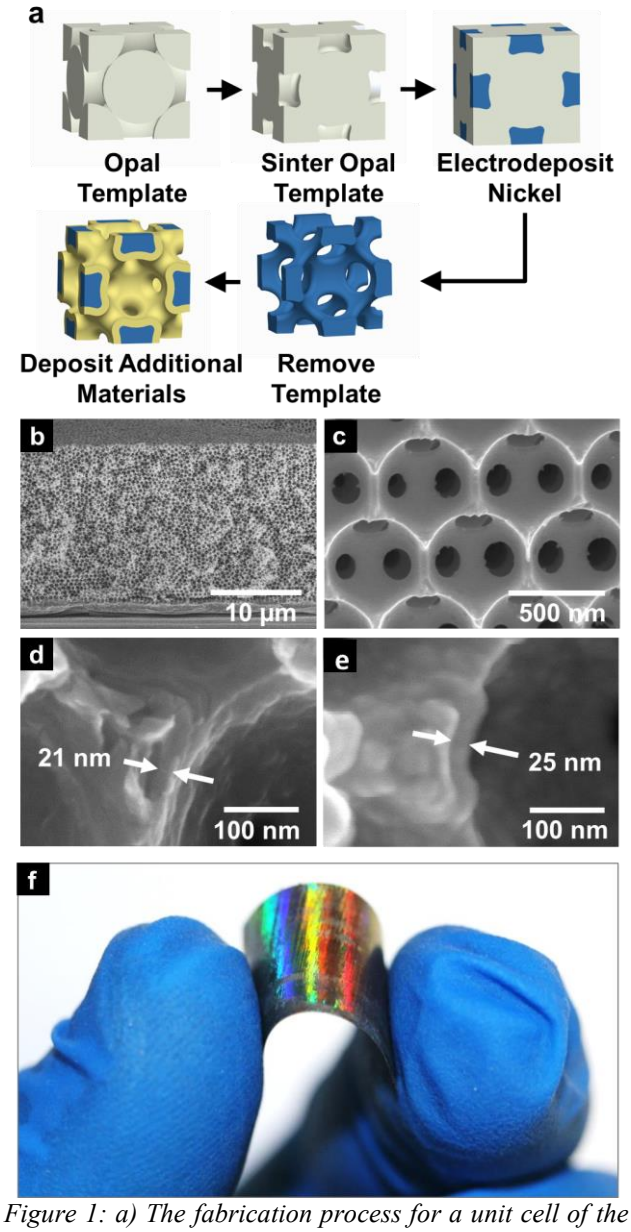

Figure 1: a) The fabrication process for a unit cell of the inverse opal nanoscale cellular solid. b-e) Cross section SEM images of nickel inverse opal nanoscale cellular solids used for mechanical testing. f) A 2 cm^2 nickel inverse opal nanoscale cellular solid with 300 nm pores grown on gold/chromium coated 20 µm thick polyimide.

Additional nickel and rhenium-nickel alloy coatings were added to the nickel inverse opals to increase the relative density and demonstrate the ability to integrate multiple chemistries into inverse opal NCS. Nickel was coated using the same commercial plating solution, but with -1.7 volts pulses for 30 seconds in between 20 second intervals of 0 amperage current for 15 – 90 cycles. The rhenium-nickel alloy coating was deposited galvanostatically versus platinum reference and counter electrodes at a 5 mA cm^{-2} current density in a pH 5 bath with 34 mM NH_4ReO_4, 93 mM $Ni(NH_2SO_3)2{\bullet}4H_2O$ and 300 mM $C_6H_8O_7$ modified from ref. [6]. NaOH was used to adjust the pH. The plating bath was immersed in silicone oil at 75°C. The plated alloy was 80 wt% percent rhenium, measured with energy-dispersive X-ray spectroscopy.

Figures 1b – 1e show SEM images of nickel inverse opal NCS with 500 nm pores fractured on the (111) plane. Figures 1b and 1c are nickel inverse opal NCS with no coating and 0.16 solid volume fractions. Figure 1d shows a nickel inverse opal NCS coated with 19 nm of additional nickel, which increased the solid volume fraction from 0.16 to 0.35. Figure 1e shows a nickel inverse opal NCS coated with 25 nm of additional rhenium-nickel alloy. The coating increased the solid volume fraction to 0.46. Figure 1f shows a 2 cm^2 nickel inverse opal NCS with 300 nm pores grown on gold/chromium-coated polyimide. The nickel inverse opal NCS on polyimide was flexible and could be bent past a 0.5 cm radius. The self-assembly technique allowed the fabrication of NCS with larger than cm^2 areas, while retaining ~10 nm control of structure and chemistry.

The inverse opal volume fraction, ε_{Ni}, and coating volume fraction, ε_{coat}, were calculated from SEM measurements of PS radius R, interconnect diameter b, and coating thickness t, along with a geometric model for the PS spheres organized in a FCC unit cell. Figure 2a shows a unit cell of an inverse opal cellular solid. The inverse opal volume is the cubic unit cell volume minus the volume of the sintered polystyrene spheres, V_{PS}. The conformally coated layer volume, V_{coat}, is the volume of a thin layer subtracted from V_{PS}. The symmetry of the FCC unit cell allows V_{coat} and V_{PS} to be calculated from the geometry of two neighboring PS spheres. Figure 2b shows the geometric model used to calculate the volume fractions. The circles with radius R represent two PS spheres in contact after opal self-assembly with an initial 0.74 volume fraction. The PS volume increases after sintering and is calculated by increasing R to R_e such that neighboring radii overlap by a length b. V_{PS} is the volume of 4 spheres of radii R_e minus the volume of 48 overlapping spherical caps of height h or

$$V_{PS} = 4\,\tfrac{4}{3}\,\pi\,{R_e}^3 - 48\,\tfrac{1}{3}\,\pi\,h^2(3\,R_e - h), \quad (1)$$

where $R_e = \sqrt{(b/2)^2 - R^2}$ and h is R_e - R. V_{coat} is the volume of spheres with radii R_c subtracted from V_{PS}. Additionally, the volume where the coating does not deposit, marked with hatching, is integrated and subtracted out, but not including the volume of the spherical cap marked by $h2$.

$$V_{coat} = V_{PS} - 4\,\tfrac{4}{3}\,\pi\,(R_c)^3 - 48\int_0^{\frac{R_c R}{R_e}} \pi\left(\frac{b}{2} - \sqrt{t^2 - x^2}\right)^2 dx + 48\tfrac{1}{3}\,\pi\,h2^2(3\,R_c - h2), \quad (2)$$

where $h2$ is $R_c\,(1 - R\,/\,R_e)$ and t is $R_e - R_c$. V_{PS} and V_{coat} normalized by the unit cell volume, $(2\,R\,\sqrt{2})^3$, calculate ε_{Ni} and ε_{coat}.

$$\varepsilon_{Ni} = 1 - \frac{V_{PS}}{(2\,R\,\sqrt{2})^3} \text{ and} \quad (3)$$

$$\varepsilon_{coat} = \frac{V_{coat}}{(2\,R\,\sqrt{2})^3}. \quad (4)$$

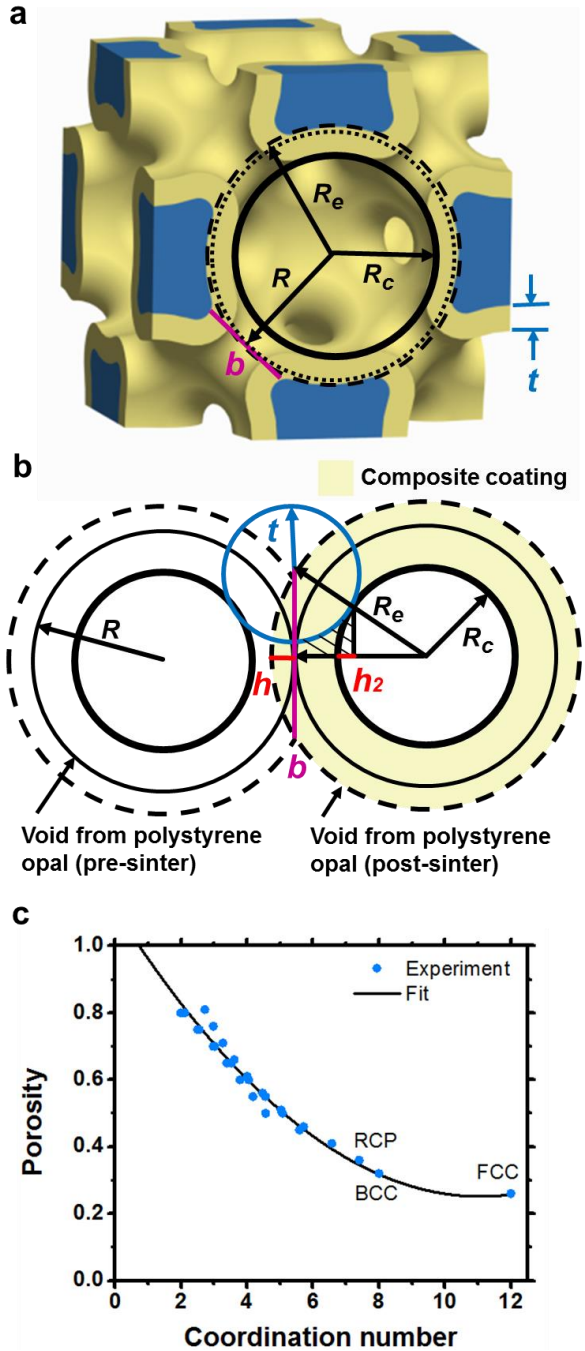

Figure 2: a) A unit cell of the inverse opal nanoscale cellular solid with important geometric parameters. b) A geometric model of the used to calculate the volume fraction of each material in the composite. c) Experimental data and curve fit relating the porosity of packed spheres to the coordination number.

Equations 3 and 4 were used to generate a sample of volumes based on the exhausted combination of the measured R, b, and t. These representative samples determine the mean and standard deviations of ε_{Ni} and ε_{coat}. R and b are measured in SEMs of the inverse opal with no coating. R is half the average distance between the center of interconnect openings, the distance from the center of b on one side of the PS void to the center of b on the other. b is the average measured interconnect diameter. t is measured by taking half the difference in the measured interconnect opening, b, before and after deposition.

Defects in the self-assembly process increased the solid volume fraction of inverse opal NCS. As the number of defects increased, the regular PS orientation degenerated into a random close packed structure (RCP) resulting in a 0.36 nickel volume fraction [7]. The volume fractions calculated in Equations 3 and 4 are corrected using the PS coordination number, CN, which is correlated to the solid volume fraction. Figure 2c shows experimental data that relates CN to porosity combined with known FCC, BCC, and RCP CNs [7]. The data is fit with $\varepsilon_{pore} = 0.007\ CN^2 - 0.155\ CN + 1.1093$, where ε_{pore} is the void volume fraction of PS spheres before sintering.

The inverse opal cellular solids were mechanically tested using micropillar compression [8]. Micropillar specimens were prepared using a focused ion beam. Annular milling in three steps resulted in cylindrical specimens of 3.6 µm diameter and 8 µm height. A final 100 nm-wide ring milling facilitated adjusting the height of the micropillars and minimizing their taper. An Agilent G200 Nanoindenter with a 10 µm diameter flat diamond punch compressed the micropillars at ~$1x10^{-4}$ s^{-1} average strain rate. The nanoindenter deformed the micropillars to a total strain of about 20%. SEM-measured micropillar diameter and height allowed the calculation of stress-strain behavior. The stress at 0.2% strain offset was used as the yield strength. The loading and unloading moduli were corrected to account for the substrate thickness [9]. The Poisson's ratio of the inverse opal cellular solids was assumed to be zero.

RESULTS AND DISCUSSION

The specific strength of inverse opal NCS resulted from the combination of two mechanical processes: porosity based weakening (size independent) and size based strengthening of the pore struts. Porosity based weakening reduced the load a NCS could support because of the reduced volume fraction of solid material and bending dominated deformation of the cellular solid struts. Size based strengthening increased the local strength of the cellular solid constituent material because of dislocation starvation in the < 1 µm strut widths [1, 10].

Yield strength, elastic moduli, and relative density measurements of fabricated inverse opal NCS with varying volume fractions deduced the effect of relative density on specific strength and stiffness. Figure 3a shows before and after SEMs of 4 µm diameter NCS micropillars used in the compression tests. The pillars were made from 500 nm diameter PS opals. Failure predominately occurred at the narrowest region of the struts along the [111] direction. The [111] direction was parallel to the micropillar axis. Figure 3b shows stress-strain curves for several NCS and bulk nickel micropillars loaded to ~0.2 strain. The cellular solid micropillars had 500 nm pores. The average yield strengths were 274, 612, and 878 MPa for cellular solids with no coating, 19 nm, and 33 nm nickel coatings, or 0.16, 0.61, and 0.88 volume fractions.

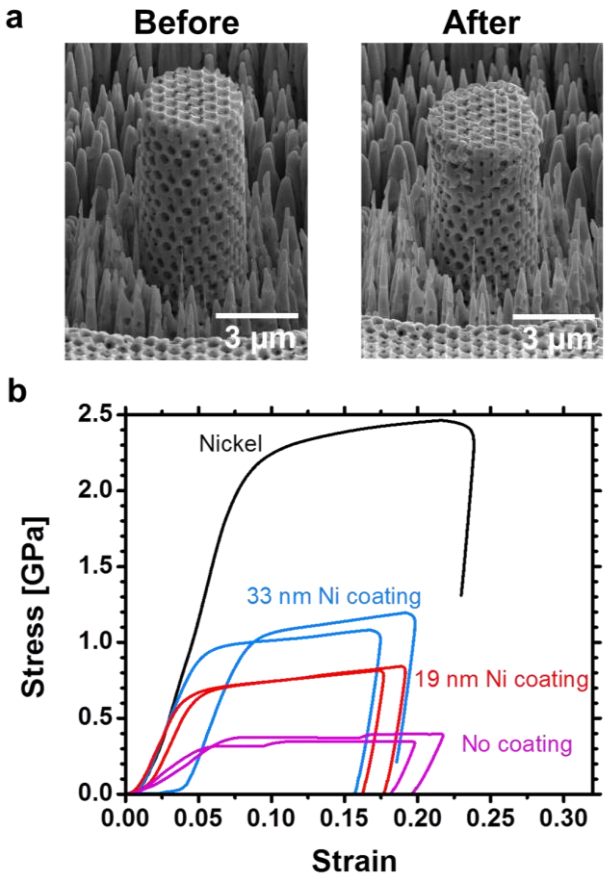

Figure 3: a) SEM images of an inverse opal nanoscale cellular solid micropillar with 500 nm pores before and after being subjected to compression testing. b) Stress-strain data for micropillars tested under compression. The nickel sample is fully dense electroplated nickel.

The strut size, solids volume fraction, and chemistry controlled the specific moduli and specific strengths of inverse opal NCS. Figure 4 shows the specific modulus versus specific strength of inverse opal NCS; select high strength titanium, nickel, aluminum, and steel alloys; and important natural materials. The specific moduli of nickel inverse opal NCS and fully dense nickel varied between 4 and 20 GPa/(Mg/m^3). The specific strengths of nickel inverse opal NCS ranged from 100 – 230 MPa/(Mg/m^3). Coating additional layers of nickel on 500 nm diameter pore cellular solids increased the solids volume fraction from 0.16 to 0.43 and increased the specific modulus from 6.2 to 9.4 GPa/(Mg/m^3). The solids volume fraction and constituent material density controlled the inverse opal NCS specific moduli. Interestingly, the specific strengths of 500 nm diameter pore inverse opal NCS remained near 200 MPa/(Mg/m^3) as additional layers of nickel were

coated. The specific strengths remained relatively constant because of the competing effects of porosity and size based strengthening. A low solids volume fraction (high porosity) reduced the cellular solid strength because of porosity based weakening, but also increased the strength of the constituent nickel because of size based strengthening, such that there was no net effect on the bulk cellular solid strength. Decreasing the pore size to 260 nm increased the specific strength of inverse opal cellular solids to 220 MPa/(Mg/m^3) because the struts were considerably smaller and therefore stronger than the 500 and 930 nm pore inverse opal NCS with similar solids volume fraction. Overall, the inverse opal cellular solids exhibited specific moduli that were similar to natural materials like bone, collagen, insect cuticles, spider silk and wood parallel to the grain. However, only the specific strength of silk exceeded the nickel inverse opal NCS. When compared to other engineered materials, nickel inverse opal NCS provide a unique combination of moderate specific stiffness similar to natural materials and high specific strengths greater than most engineering alloys.

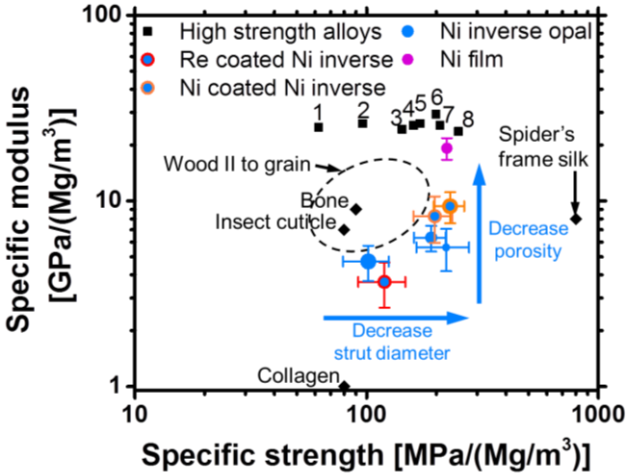

Figure 4: An Ashby plot comparing the specific modulus and specific strength of nickel coated (orange) and rhenium coated (red) nickel inverse opal nanoscale cellular solids to other high strength materials. Bulk electrodeposited nickel is shown in pink. Common Ti, Al, Ni, and Fe high strength alloys are labeled 1 – 8: 1 - CP Ti, 2 - 2024-T4, 3 - Inconel 718, 4 - 4143 steel, 5 - 7075-T6, 6 - HSSS steel, 7 - Ti-6Al-4V, 8 - Ti-10V-2Fe-3Al.

CONCLUSION

In conclusion, we used self-assembly of µm sized particles to fabricate nickel and rhenium nanocomposite inverse opal NCS with controllable porosity and pore size, which allowed specific moduli between 4 and 20 GPa/(Mg/m^3) and specific strengths up to 230 MPa/(Mg/m^3). The inverse opal NCS had specific strengths greater than most high strength alloys, yet deformed primarily by bending, resulting in specific stiffness similar to natural materials. The self-assembly based fabrication overcame the maximum sample size restrictions of other fabrication technologies, enabling macroscopic NCS that can be integrated into engineered devices [11].

ACKNOWLEDGEMENTS

This research was supported in part by the Department of Energy Office of Science Graduate Fellowship Program (DOE SCGF), made possible in part by the American Recovery and Reinvestment Act of 2009, administered by ORISE-ORAU under contract no. DE-AC05-06OR23100.

REFERENCES

[1] Z. Shan, R. K. Mishra, S. S. Asif, O. L. Warren, and A. M. Minor, "Mechanical annealing and source-limited deformation in submicrometre-diameter Ni crystals," Nature Materials, vol. 7, pp. 115-119, 2008.

[2] L. R. Meza, S. Das, and J. R. Greer, "Strong, lightweight, and recoverable three-dimensional ceramic nanolattices," Science, vol. 345, pp. 1322-1326, September 12, 2014 2014.

[3] P. Fratzl and R. Weinkamer, "Nature's hierarchical materials," Progress in Materials Science, vol. 52, pp. 1263-1334, 2007.

[4] J. Bauer, S. Hengsbach, I. Tesari, R. Schwaiger, and O. Kraft, "High-strength cellular ceramic composites with 3D microarchitecture," Proceedings of the National Academy of Sciences, February 3, 2014 2014.

[5] X. Zheng, H. Lee, T. H. Weisgraber, M. Shusteff, J. DeOtte, E. B. Duoss, J. D. Kuntz, M. M. Biener, Q. Ge, J. A. Jackson, S. O. Kucheyev, N. X. Fang, and C. M. Spadaccini, "Ultralight, ultrastiff mechanical metamaterials," Science, vol. 344, pp. 1373-1377, June 20, 2014 2014.

[6] A. Naor, N. Eliaz, and E. Gileadi, "Electrodeposition of rhenium–nickel alloys from aqueous solutions," Electrochimica Acta, vol. 54, pp. 6028-6035, 2009.

[7] J. van de Lagemaat, K. D. Benkstein, and A. J. Frank, "Relation between Particle Coordination Number and Porosity in Nanoparticle Films: Implications to Dye-Sensitized Solar Cells," The Journal of Physical Chemistry B, vol. 105, pp. 12433-12436, 2001.

[8] M. D. Uchic, P. A. Shade, and D. M. Dimiduk, "Plasticity of Micrometer-Scale Single Crystals in Compression," Annual Review of Materials Research, vol. 39, pp. 361-386, 2009.

[9] H. Fei, A. Abraham, N. Chawla, and H. Jiang, "Evaluation of Micro-Pillar Compression Tests for Accurate Determination of Elastic-Plastic Constitutive Relations," Journal of Applied Mechanics, vol. 79, pp. 061011-061011, 2012.

[10] J. R. Greer, W. C. Oliver, and W. D. Nix, "Size dependence of mechanical properties of gold at the micron scale in the absence of strain gradients," Acta Materialia, vol. 53, pp. 1821-1830, 2005.

[11] J. H. Pikul, Z. Dai, X. Yu, H. Zhang, T. Kim, P. V. Braun, and W. P. King, "Micromechanical devices with controllable stiffness fabricated from regular 3D porous materials," Journal of Micromechanics and Microengineering, vol. 24, p. 105006, 2014.

CONTACT

*W.P. King, tel: +1-217-2443864; wpk@illinois.edu